Short- and medium-range order in a $Zr_{73}Pt_{27}$ glass: Experimental and simulation studies

S. Y. Wang,[1,2] C. Z. Wang,[2,3] M. Z. Li,[4,2] L. Huang,[2] R. T. Ott,[3] M. J. Kramer,[3] D. J. Sordelet,[3] and K. M. Ho[2]
[1]*Department of Optical Science and Engineering, State Key Laboratory for Advanced Photonic Materials and Devices, Fudan University, Shanghai 200433, China*
[2]*Ames Laboratory–U.S. Department of Energy and Department of Physics and Astronomy, Iowa State University, Ames, Iowa 50011, USA*
[3]*Materials Science and Engineering, Ames Laboratory–USDOE, Ames, Iowa 50011, USA*
[4]*Department of Physics, Renmin University of China, Beijing 100872, China*
(Received 23 April 2008; revised manuscript received 29 September 2008; published 21 November 2008)

The structure of a $Zr_{73}Pt_{27}$ metallic glass, which forms a Zr_5Pt_3 (Mn_5Si_3-type) phase having local atomic clusters with distorted icosahedral coordination during the primary crystallization, has been investigated by means of x-ray diffraction and combining *ab initio* molecular-dynamics (MD) and reverse Monte Carlo (RMC) simulations. The *ab initio* MD simulation provides an accurate description of short-range structural and chemical ordering in the glass. A three-dimensional atomistic model of 18 000 atoms for the glass structure has been generated by the RMC method utilizing both the structure factor $S(k)$ from x-ray diffraction experiment and the partial pair-correlation functions from *ab initio* MD simulation. Honeycutt and Andersen index and Voronoi cell analyses, respectively, were used to characterize the short- and medium-range order in the atomistic structure models generated by *ab initio* MD and RMC simulations. The *ab initio* results show that an icosahedral type of short-range order is predominant in the glass state. Furthermore, analysis of the atomic model from the constrained RMC simulations reveals that the icosahedral-like clusters are packed in arrangements having higher-order correlations, thus establishing medium-range topological order up to two or three cluster shells.

DOI: 10.1103/PhysRevB.78.184204 PACS number(s): 61.43.Fs, 61.05.cp, 61.43.Bn, 61.20.Gy

I. INTRODUCTION

The local atomistic structures of liquid and amorphous phases play an important role in dictating the transformation pathways in metallic alloy systems.[1–5] Amorphous, crystalline, or quasicrystalline phases that have short-range order (SRO) and medium-range order (MRO) similar to their corresponding liquid structures have been suggested to possess smaller interfacial free energies between their liquid and solid phases compared to phases with dissimilar structures.[6] This SRO and MRO can be an influential factor not only in the selective nucleation of certain structures among many competing pathways, but also in avoiding crystallization to form a glass when rapidly cooling liquid metallic alloys.[7]

Nanometer-sized icosahedral quasicrystals have been observed in a number of Zr-based alloys with noble metals.[8–13] Since most of them are formed as a primary crystallization phase from the glass state, a structural correlation between the local structures in amorphous state and the icosahedral phase has been suggested from these experiments.[14–16] But a comprehensive understanding is still lacking because most experimental evidence is still limited to pair-distribution information, although some progress in measurement of species specific local coordination from extended x-ray absorption fine structure (EXAFS) has been reported.[5] Because the amorphous state is normally generated from the liquid, in order to help us understand why icosahedral phase formation is so prevalent in Zr-based systems, we investigated the local atomic structures from liquid to amorphous states in one specific alloy composition within the family of near-eutectic binary Zr-Pt glasses, which Lee *et al.*[17] showed to exhibit a strong dependence of structure and crystallization behavior on composition.

Unlike crystalline systems, where the average atomic positions are described by their translational and rotational symmetries, the structure of liquid or amorphous systems can only be described statistically. For instance, although diffraction experiments provide an accurate description of the one-dimensional (1D) pairwise correlations, they are insufficient for obtaining the higher-order correlations necessary to describe a three-dimensional (3D) structure. Consequently, these experiments need to be coupled with short-range many-body correlations from accurate atomistic simulations to yield a thermodynamically self-consistent three-dimensional structural model. There is also an increasing consensus that accurate descriptions of liquid and amorphous structures need to go beyond the average packing of nearest neighbors and incorporate clusters of atoms which may have medium-range chemical and structural ordering.[18–21] Therefore, knowledge of the 3D structures of liquid and amorphous alloys at the atomistic level is required for a better understanding of short- and medium-range correlations, thermodynamic stability, and mechanisms for phase selection and transformations. In this paper, we combine experimental x-ray diffraction data with an approach that brings together *ab initio* molecular-dynamics (MD) simulations as well as reverse Monte Carlo (RMC) simulations to study the structure of a $Zr_{73}Pt_{27}$ glass. A reliable 3D atomistic structure model has been generated through this combined approach that allows us to gain a more detailed understanding of the topological framework of the SRO and the MRO in this glass system.

This paper is arranged as follows. The experimental and computational details will be presented in Sec. II. The results obtained from our experiment and simulations will be presented and discussed in Sec. III. Specifically, we first de-

scribe the total scattering and pair-correlation functions obtained from experiment and simulations. Next, we present description of the SRO from the *ab initio* MD simulations and build upon that to discuss the SRO and the MRO details provided from the RMC models. Finally, concluding remarks appear in Sec. IV.

II. EXPERIMENTAL AND SIMULATION METHODS

A. X-ray diffraction

The $Zr_{73}Pt_{27}$ glass samples were prepared by first arc melting buttons of high-purity Zr and Pt and then subsequently quenching the molten alloy by melt spinning ribbons onto a rotating Cu wheel. Details on preparation are given elsewhere.[17] High-energy transmission synchrotron x-ray diffraction (HEXRD) studies of the as-spun ribbons were performed at the 6-ID-D MUCAT beam line of the Advanced Photon Source at Argonne National Laboratory. A monochromatic x-ray beam with an energy of 98.685 keV ($\lambda = 0.125\,636$ Å) was employed for the experiments performed in transmission geometry. A MAR 345 digital image plate with a 100×100 μm^2 pixel size was positioned 235 mm downstream from the samples to record the two-dimensional (2D) scattering pattern over a k range up to 30 $Å^{-1}$, where k is the scattering vector ($k = 4\pi \sin\theta/\lambda$). The distance between the sample and 2D detector was determined by fitting the pattern from NIST Si-standard 640C using the FIT2D software.[22] The observed intensities were obtained at room temperature and corrected for absorption, background, multiple scattering, polarization, and sample geometry using standard procedures.[23] The coherent scattering data were converted to the total structure function $S(k)$ according to

$$S(k) = 1 + \frac{I(k) - \sum_{i=1}^{n} a_i |f_i(k)|^2}{\left| \sum_{i=1}^{n} a_i f_i(k) \right|^2}, \tag{1}$$

where $I(k)$ is the coherently scattered portion of the total intensity, a_i is the atomic proportion of each element, and $f_i(k)$ is the k-dependent scattering factor for each element.

The pair-correlation function (PCF) $g(r)$ was calculated by Fourier transforming the total scattering function as follows:

$$g(r) = \frac{\rho(r)}{\rho_o} = 1 + \frac{1}{4\pi r \rho_o} \left\{ \frac{2}{\pi} \int_0^\infty k[S(k) - 1] \sin(kr) dk \right\}, \tag{2}$$

where $\rho(r)$ is the atomic density at a distance r from an average atom located at the origin and ρ_0 is the average atomic density of the material as determined by *ab initio* MD simulation in Sec. II B.

B. *Ab initio* molecular-dynamics simulations

Ab initio MD simulations of $Zr_{73}Pt_{27}$ were performed using the Vienna *ab initio* simulation package (VASP).[24–28] The system consisted of 100 atoms (73 atoms of Zr and 27 atoms of Pt) in a cubic box with periodic boundary conditions. A plane wave basis with energy cutoff of 230.2 eV is used. The interaction between the ions and electrons is described by the projector augmented-wave (PAW) method. In the PAW potential, $4s4p5s4d$ and $5d6s$ orbitals of Zr and Pt, respectively, are treated as valence orbitals. The MD simulations started with the atoms placed at random positions in the cubic box at 3000 K, which is well above the melting temperature ($T_m \sim 1800$ K) of this composition. Such a high temperature was achieved in order to avoid any memory effects from the initial configuration. Only the Γ point was used to sample the Brillouin zone of the supercell. Once the *ab initio* forces are evaluated, a canonical ensemble MD simulation with constant number of particles, constant volume, and constant temperature (NVT) was performed using a Nosé-Hoover thermostat to control the temperature.[29,30] The atomic number density was initially determined by a linear combination of the densities for pure liquid Zr and Pt. A liquid structure of $Zr_{73}Pt_{27}$ at 3000 K was obtained after 1000 time steps of MD simulation. Afterward the system was cooled from 3000 to 2500, 2200, and 1850 K at a uniform cooling rate of 0.2 K/step. At each temperature, the simulation was further carried out for another 1000 time steps (3 ps) to collect the configurations for statistical analysis of the structures and properties of the liquid. The liquid was then cooled down to 0 K at a constant cooling rate of 0.2 K/step to obtain the glassy state. The density of the glass structure obtained from the cooling procedure was further optimized by calculating the total energy of the amorphous structure as a function of the volume of the cubic box, which gives an optimum atomic number density of 49.64 atom/nm^3 at essentially zero pressure. The structural properties of the amorphous are then calculated by performing the statistical averages over 1000 MD steps at 200 K.

C. Reverse Monte Carlo simulations

Although *ab initio* MD simulations can provide a great deal of insight into the short-ranged structural and chemical order in metallic liquid and glass alloys, atomistic 3D models with several thousand atoms or more are necessary for studying higher-order and longer-range correlations in these disordered systems. Reverse Monte Carlo modeling has been a widely used method to generate a three-dimensional structure of several thousand atoms by matching the $S(k)$ or $g(r)$ of the structure model with that obtained from experimental measurements.[5,31,32] Although the RMC technique has some advantages including not requiring interatomic potentials, some caution must be exercised with this 1D-to-3D inverse approach because the nonuniqueness of its solutions results in the most disordered model fit to the diffraction data.[33,34] The rigor of this approach can be greatly improved by incorporating additional scattering data or local SRO information (e.g., partial pair-correlation functions from *ab initio* MD simulations) as constraints to the statistical sampling of the topological order probed by diffraction. In the current study, we adopted such a constrained RMC approach. Our RMC

simulations were performed with 18 000 atoms matching the stoichiometry of the $Zr_{73}Pt_{27}$ alloy. The simulations were started with the atoms randomly placed in a cubic box. Periodic boundary conditions were applied and the box length was selected to fit the atomic density of the glass state determined by the *ab initio* MD simulation described above. In addition to the experimentally measured $S(k)$, the partial pair-correlation functions from the *ab initio* MD simulations were also used as constraints to determine the 3D atomistic structure model for the glass phase of $Zr_{73}Pt_{27}$. Our approach is different from that of Sheng *et al.*,[5] whose RMC simulations were constrained with species specific local coordination data obtained from EXAFS measurements while fitting to an $S(k)$ obtained from synchrotron x-ray diffraction data.

D. Structure analysis based on simulation models

Reliable atomistic models for amorphous and liquid alloys enable us to perform various structural analyses. Using the atomic coordinates from the *ab initio* MD and RMC simulations, the total pair-correlation function $g(r)$ can be calculated by

$$g(r) = \rho_0^{-2}\left\langle \sum_i \sum_{j\neq i} \delta(\mathbf{r}_i)\,\delta(\mathbf{r}_j - \mathbf{r})\right\rangle. \tag{3}$$

The partial pair-correlation functions $g_{ij}(r)$ can also be calculated when the density in Eq. (3) is set to be the corresponding partial density $\rho_{ij}=\rho_0\sqrt{a_i a_j}$, where i and j denote the elements in the alloy and a_i and a_j are their concentrations. The total structure factor $S(k)$ from the simulations were obtained using the Faber-Ziman formalism.[35] $S(k)$ is derived from the three partial structure factors $S_{ij}(k)$, the scattering factors f_i and f_j, and atomic concentration of the elements a_i and a_j in the alloys,

$$S(k) - 1 = \frac{a_i^2 f_i^2[S_{ii}(k)-1] + 2a_i a_j f_i f_j[S_{ij}(k)-1] + a_j^2 f_j^2[S_{jj}(k)-1]}{(a_i f_i + a_j f_j)^2}. \tag{4}$$

The scattering factors f_i and f_j are k dependent for x-rays and are obtained from tabulated data.[36] The Faber-Ziman partial structure factors $S_{ij}(k)$ are related to the partial pair-correlation functions $g_{ij}(r)$ by

$$S_{ij}(k) = 1 + 4\pi\rho_{ij}\int_0^\infty [g_{ij}(r)-1]\frac{\sin(kr)}{kr}r^2 dr. \tag{5}$$

Using the atomic coordinates from the MD and RMC simulations, information about higher-order correlations in the liquid and glass alloy may also be obtained in addition to the pair-correlation function $g(r)$. The SRO and statistical distribution of polytetrahedral clusters in the 3D atomistic structure models can also be analyzed by several commonly used methods, including Honeycutt and Andersen (HA) indices,[37] Voronoi tessellation method,[38,39] and bond-orientational order (BOO) parameters,[40] as outline briefly below.

To begin with, HA indices provide topological information about the local structure. In this technique pairs of atoms can be classified by the relationship among their neighbors with four integer indices. Ganesh and Widom[41,42] simplified the HA analysis by assigning a set of three indices to each bond. The first index is 1 if the root pairs are bonded (i.e., separation less than or equal to R_{cut}). The second index is the number of near-neighbor atoms common to the root pairs and the third index gives the number of near-neighbor bonds between these common neighbors. In general, 142's are characteristic of close-packed structures such as fcc and hcp and 143's are characteristic of distorted icosahedrons. The 144-type and 166-type pairs characterize a body-centered-cubic-like local structure, while the 155 type is characteristic of icosahedral order. For instance, local order built on a 13-atom icosahedron leads to the occurrence of 155 and 132 pairs. The 154 and 143 pairs are formed when a regular 155 structure is deformed. The 155-type pair, corresponding to two neighboring atoms with five common neighbors that form a pentagon of near-neighbor contacts, can be regarded as five tetrahedra organized around a common neighboring pair. The deviation of the 154 pair from the 155 pair is very small, and as such it may be viewed as a deformed icosahedron. The 143-type pair can be regarded as four tetrahedra with some distortion.

Voronoi clusters (VCs) are defined as closed polyhedra built up from face-sharing tetrahedral with a common central atom. A VC is an analog for a disordered structure, as in the well-known Wigner-Seitz cell in crystals. In three-dimensional space, a VC is a convex polyhedron formed by certain planes drawn perpendicular to the intercenter vectors at their midpoints. We use the Voronoi index $\langle n_3, n_4, n_5, n_6, \ldots\rangle$, where n_i denotes the number of i-edged faces of the Voronoi polyhedron around a central atom, to designate the character of the local atomic cluster surrounding that atom. For example, an index $\langle 0,0,12,0\rangle$ indicates that the polyhedron has only 12 pentagonal faces, which is the characteristic of a 13-atom icosahedra cluster.

The BOO parameter analysis introduced by Steinhardt *et al.*[40] provides additional information on the local structure of a regular or disordered structure. A set of order parameters expressed in terms of spherical harmonics $Q_{lm}(r) = Y_{lm}[\theta(r),\varphi(r)]$ is associated with the orientation regardless of the bond length of each pair. To account for equivalent structures that are oriented differently, the rotationally invariant combination is used,

$$Q_l = \sqrt{\frac{4\pi}{2l+1}\sum_{m=-l}^{l}|\bar{Q}_{lm}|^2} \tag{6}$$

and the third-order invariants are defined as

$$W_l = \sum_{\substack{m_1,m_2,m_3 \\ m_1+m_2+m_3=0}} \begin{pmatrix} l & l & l \\ m_1 & m_2 & m_3 \end{pmatrix} \bar{Q}_{lm_1}\bar{Q}_{lm_2}\bar{Q}_{lm_3}, \tag{7}$$

where the coefficients $\left(\begin{smallmatrix} l & l & l \\ m_1 & m_2 & m_3 \end{smallmatrix}\right)$ are the Wigner $3j$ indices. It is standard to define a normalized quantity

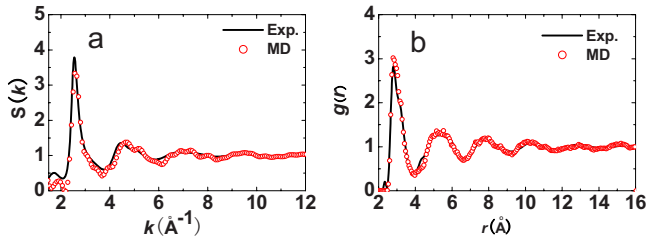

FIG. 1. (Color online) (a) Total structure factor $S(k)$ and (b) pair-correlation function of $Zr_{73}Pt_{27}$ metallic glass obtained from the *ab initio* MD simulations compared with those from HEXRD measurements.

$$\hat{W}_l \equiv \frac{W_l}{\left(\sum_m |Q_{lm}|^2\right)^{3/2}} \tag{8}$$

which, for a given l, is independent of the magnitudes of $\{Q_{lm}\}$.

Different structures are characterized by $\hat{W}_l$'s of different intensities. In particular, we monitored the $\hat{W}_6$ cubic invariant. This is the most sensitive indicator for icosahedral symmetry. For an isolated 13-atom cluster, $\hat{W}_6 = -0.169$ and -0.013 for icosahedral and face-centered cubic structures, respectively.

III. RESULTS AND DISCUSSION

A. Structure factor and pair-correlation functions

The structure factor obtained from the HEXRD measurement is presented in Fig. 1(a). It clearly shows that this sample is amorphous and no indication of Bragg peaks is visible. A prepeak at scattering vector k near 1.7 $Å^{-1}$ is present. The presence of a prepeak has been reported for amorphous Zr-based binary alloys containing Au, Pd, and Pt (Ref. 43) and was proposed to result from strong chemical short-range order around the noble-metal atoms, arising in part from their large negative heats of mixing with Zr. The maximum of the first and the second peaks is at 2.54 and 4.46 $Å^{-1}$, respectively, and oscillations are clearly seen up to 20 $Å^{-1}$. A shoulder on the right-hand side of the second oscillation is observed for the measured $S(k)$ of the amorphous $Zr_{73}Pt_{27}$. This shoulder may be a characteristic of a particular SRO. For example, such features in supercooled liquids and metallic glasses have been identified as a signature of icosahedral SRO (ISRO) from the theoretical work of Sachdev and Nelson[44] and were recently reported in quasicrystal-forming alloy melts[45] and deeply undercooled metallic liquids of Ni, Fe, and Zr.[46]

The experimental pair-correlation function $g(r)$ of $Zr_{73}Pt_{27}$ metallic glass as shown in Fig. 1(b) is obtained by Fourier transformation of the measured total structure factor $S(k)$ using Eq. (2). A small prepeak at 2.34 Å is probably a truncation ripple caused by the Fourier transforming of the experimental data due to the finite k space. The first main peak at 2.8 Å is very well separated from the remainder of the $g(r)$ data; and this, in principle, makes it possible to accurately calculate the coordination number N, which is defined as the average number of atoms in the nearest-neighbor shell. Performing the appropriate integration of the $g(r)$ up to 3.94 Å, the value of coordination number $N=12.6$ is obtained. Note that the first peak of $g(r)$ exhibits a very distinct shoulder around 3.0 Å which is about the nearest-neighbor distance between a pair of Zr atoms. The appearance of this shoulder can be attributed to the fact that Zr atoms have smaller scattering intensity than Pt atoms in the x-ray diffraction experiment. The second peak of $g(r)$ is located at 5.44 Å and is much broader than the first peak, indicating that this longer-range assemblage represents a convolution of atomic pair correlations, as discussed below.

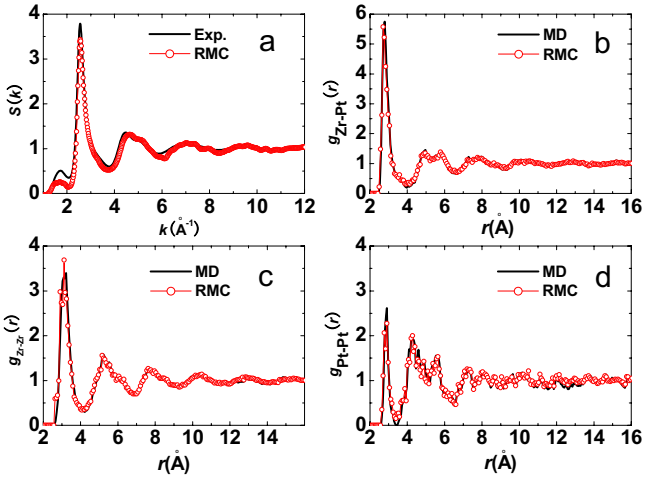

FIG. 2. (Color online) (a) Structure factor $S(k)$ of amorphous $Zr_{73}Pt_{27}$. $S(k)$ from RMC is compared to that from x-ray diffraction experiment. Partial pair-correlation functions $g_{ij}(r)$ from MD and RMC simulations for (b) Zr-Pt, (c) Zr-Zr, and (d) Pt-Pt.

Using the atomic coordinates from the *ab initio* MD simulation, the total structure factor was calculated from Eqs. (4) and (5). The total pair-correlation function $g(r)$ can also be calculated by the Fourier transformation of $S(k)$ spectrum,

$$g(r) = 1 + \frac{1}{2\pi^2 \rho r}\int_0^{k_{\max}} k[S(k)-1]\sin(kr)dk. \tag{9}$$

The calculated structure factor and total pair-correlation function for the amorphous $Zr_{73}Pt_{27}$ are compared with the experimental results in Figs. 1(a) and 1(b), respectively. Both the peak positions of $S(k)$ and $g(r)$ and the shoulder in the right-hand side of the first peak of $g(r)$ from the simulation agree well with that in experiment. This agreement indicates that the structure model obtained from the *ab initio* MD simulation is physically meaningful and the partial pair-correlation functions obtained from the simulation, which are impossible to measure from a single fixed-energy experiment, are reliable for providing useful insights into the short-ranged structure and chemical order in the $Zr_{73}Pt_{27}$ glass alloy. In addition, the partial pair-correlation functions from the *ab initio* MD simulation can serve as important constraints to the RMC modeling of the glass structures using a much larger number of atoms.

As shown in Fig. 2(b), the partial pair-correlation function

TABLE I. Coordination numbers N calculated from MD and RMC simulations for $Zr_{73}Pt_{23}$ glass.

	Total	Zr-Pt	Zr-Zr	Pt-Pt	Pt-Zr
MD	13.02	3.68	9.95	1.44	9.95
RMC	12.83	3.60	9.75	1.69	9.73

between Zr and Pt $g_{\text{Zr-Pt}}(r)$ in amorphous $Zr_{73}Pt_{27}$ exhibits a first sharp peak at 2.78 Å. The second broad peak consists of two small peaks. It is these two small peaks that combine to broaden the second peak of measured total $g(r)$ around 5.44 Å. In the partial pair-correlation function between the Zr-Zr atoms $g_{\text{Zr-Zr}}(r)$ [Fig. 2(c)] the first peak is around 3.19 Å, which is very close to the experimental value of 3.15 Å reported for supercooled pure Zr.[46] The partial pair-correlation functions for Pt atoms $g_{\text{Pt-Pt}}(r)$ is shown in Fig. 2(d). The statistics for $g_{\text{Pt-Pt}}(r)$ is poor because the number of Pt atoms is small. Nevertheless, the first peak position located around 2.8 Å can be clearly seen. This value is larger than that of pure liquid Pt at 2053 K (2.7 Å).[47] As shown in Fig. 2, the 3D atomistic structure from the RMC simulation accurately reproduces all the partial pair-correlation functions from the *ab initio* MD simulation. In addition, as shown in Fig. 2(a), the RMC model also reproduces the structure factor $S(k)$ from the x-ray diffraction experiment, with the exception of the prepeak at $k \sim 1.7$ Å^{-1}, where the intensity from the RMC model is smaller than that from the experiment. It should be noted that inclusion of the partial pair-correlation functions from *ab initio* MD simulations as constraints to the RMC simulation is very crucial for obtaining a reliable glass structure model. We found that structure models fitted to the $S(k)$ from experiment without these constraints give very different partial pair-correlation functions. Some of which were physically unrealistic (e.g., Pt-Pt bonds at shorter distances than Zr-Zr atoms) and yielded very different short-ranged chemical orders, as compared to the *ab initio* MD simulation results.

B. Short-range order from *ab initio* MD simulations

Before discussing the possible MRO in the $Zr_{73}Pt_{27}$ glass using the atomistic model from the RMC simulation, let us first look at the SRO based on the *ab initio* MD simulation results. Note, however, that the results for the coordination number from the RMC model are also included in this subsection to compare with the results from the *ab initio* MD simulations. Such comparison, particularly the latter, can provide a more comprehensive somewhat independent picture of the similarities and differences between the MD and RMC models since these properties were *not* explicitly included in the RMC fitting to determine the atomistic model.

Using the partial pair-correlations as shown in Fig. 2, coordination numbers N and chemical distribution around both Zr and Pt atoms (i.e., partial coordination number) can be determined. The coordination number from the *ab initio* MD and RMC atomistic models are listed in Table I. The total coordination number calculated from both the *ab initio* MD and RMC models is about 13.0, which is slightly larger than

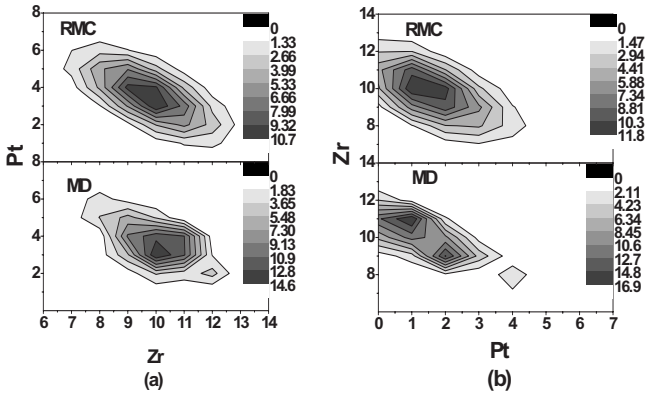

FIG. 3. Distribution of local coordination numbers in glass $Zr_{73}Pt_{27}$ calculated from the MD and RMC models. (a) Zr-centered distribution functions and (b) Pt-centered distribution functions.

that (12.6) from the experiment. All the partial coordination numbers, with the exception of Pt-Pt, calculated from MD are slightly larger than those from the RMC model. This may be attributed to the lower number of Pt atoms in our MD simulated $Zr_{73}Pt_{23}$ alloy.

In order to see the chemical ordering around the Zr and Pt atoms more clearly, the partial coordination number distribution around the Zr and Pt atoms was calculated and shown in Fig. 3. While the coordination number distribution around Zr atoms [Fig. 3(a)] shows a peak about Zr$\sim$10 and Pt$\sim$3, the distribution around the Pt atoms the MD simulation exhibits two peaks: the bigger one at Zr$\sim$11 and Pt$\sim$1 and the smaller one at Zr$\sim$9 and Pt$\sim$2. In the RMC model, there is one broad peak around Zr$\sim$10 and Pt$\sim$1.5. On average, each Pt atom has $\sim$1.5 Pt atoms and $\sim$10.5 Zr atoms as its nearest neighbors, while each Zr atom has $\sim$10 Zr and $\sim$3 Pt neighbors in the glass structure obtained from the *ab initio* MD simulation. The results from the RMC model are similar to those from the *ab initio* MD model, although the distribution in the RMC model seems broader than that of the MD model, as depicted in Fig. 3. This may be attributable to the fact that the RMC model has many more atoms and can sample a larger phase space.

The preceding discussion explains how atoms are coordinated within the SRO of the $Zr_{73}Pt_{27}$ glass, and the next step is to formulate a topological description of the higher-order atomic correlations that extend beyond the first nearest-neighbor shell. Specifically, in discussing the structure of glass and liquid materials, it is useful to consider the types of structural order that can exist in such materials at various length scales. For example, SRO can be regarded as given by structural correlations in the range of 2–5 Å, MRO in the range of 5–20 Å, and long-range order (LRO) structure at distances more than 20 Å.[48] Before discussing the MRO in the glass model from the RMC simulation, let us first examine some local cluster structures from the model generated by the *ab initio* MD simulations. Figures 4(a) and 4(b) show some typical clusters of icosahedra centered with Zr and Pt atoms, respectively, in the structure model obtained by *ab initio* MD simulation. The size of a single icosahedral cluster lies in a range of 2–5 Å, which is simply a structure with SRO. However, some icosahedra are found to connect

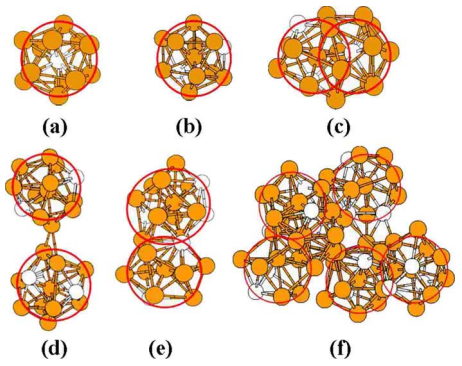

FIG. 4. (Color online) Icosahedral clusters of metallic glass alloy ZrPt from MD simulation. (a) Pt-centered, (b) Zr-centered, (c) interpenetrating icosahedra, (d) vertex-connected, (e) Face-sharing icosahedra, and (f) Medium-range order made up of icosahedra in glass $Zr_{73}Pt_{27}$. Yellow and white spheres denote Zr and Pt atoms, respectively.

with each other in the glass structure. Figures 4(c)–4(e) shows some possible icosahedra, such as interpenetrating icosahedra, vertex-connected, and face-sharing icosahedra, which are made up of two icosahedra. For example, in Fig. 4(c), two 13-atom clusters are interpenetrating with each other and the number of common atoms is as large as seven. The examples of vertex-connected and face-sharing icosahedra are shown in Figs. 4(d) and 4(e), respectively. Figure 4(f) shows seven icosahedra (six Zr centered and one Pt centered) connected to each other to form structure on a length scale associated with the MRO in the $Zr_{73}Pt_{27}$ glass. Similar atomic configurations with interpenetrating and face-sharing icosahedra have also been observed by Sheng *et al.*[5] in $Zr_{84}Pt_{16}$ metallic glass. Additional details about how the clusters in our glass arrange themselves to constitute the MRO in the glass are discussed in Sec. III C based on the RMC simulations.

It is also interesting to investigate how the SRO in the glass develops during cooling from the liquid in the *ab initio* MD simulations. For this purpose, we have performed HA index analysis for the liquid and glass structures using the atomistic coordinates from the MD simulation. The results of liquid at 3000, 2500, 2200, and 1850 K have been obtained by averaging over 3 ps of the MD simulations at each temperature after the liquid structures have been well equilibrated at the given temperature. For the glass state, the MD simulation is performed at 200 K and also averaged over 3 ps. In order to determine the cutoff distance for the HA index calculation at different temperatures, we have calculated the pair-correlation function $g(r)$ of the glass and the liquids at different temperatures and found that the first minima of $g(r)$ at different temperatures are essentially the same at ~3.94 Å. Therefore a common r_{cut}=3.94 Å is used for the calculations of HA index at all temperatures. The calculated numbers of selected HA pairs for liquid and glass of $Zr_{73}Pt_{27}$ from the MD simulation are shown in Fig. 5. It can be seen from Fig. 5 that the $Zr_{73}Pt_{27}$ glass consists mainly of 15's and 14's HA pairs. The sum of the icosahedral and distorted icosahedral related pairs (i.e., 155, 154, and 143 pairs) for the amorphous from the MD simulation constitutes more

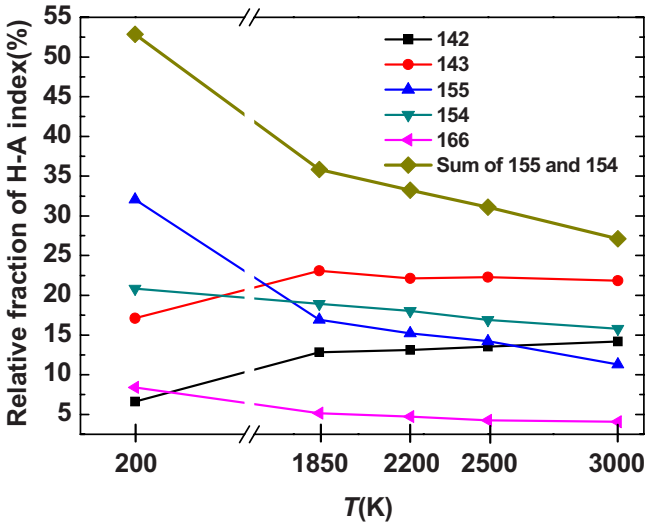

FIG. 5. (Color online) Population of the HA index in the liquid and glass $Zr_{73}Pt_{27}$ from the *ab initio* MD simulation when the sample is cooled from 3000 K liquid to the amorphous state at 200 K.

than 63% of the total pairs. This indicates that the SRO of the glass state is dominated by icosahedral and distorted icosahedral inherent structures due to the preponderance of the 15's and 143's bonded pairs. It is also interesting to note that the population of the 15's pairs increases monotonically as the structure is cooled down from the high-temperature liquid. This behavior clearly indicates the development of icosahedral-like ordering from the liquid as the system is cooled. The development of icosahedral ordering upon cooling from the liquid is also observed by Voronoi cell analyses.

C. Short- and medium-range order from the RMC model

From Figs. 1–3 together with Table I, we can see that the results from *ab initio* MD simulation agree well with experimental measurement; moreover, the results from the RMC simulation are also in reasonably good agreement with the *ab initio* MD results. Collectively, these indicate that the atomistic structure model from our RMC simulation is a reasonable representation of the amorphous $Zr_{73}Pt_{27}$ structure. Using the 18 000-atom RMC structure model, we performed additional structural analyses in order to gain further insight into the nature of the MRO in this glass alloy.

Figure 6 displays the fraction of the 14 most abundant types of polyhedra from the Voronoi analysis of the RMC model. The x axis is arranged according to the coordination numbers (CN) of the clusters, with CN increases from the left to right. For the same CN, the larger fraction of the VC is in the left. The clusters with lower CN are mostly Pt-centered clusters while the Zr-centered clusters have higher CN as one can see from Fig. 6. The most favored clusters are $\langle 0,3,6,4\rangle$, followed by $\langle 0,1,10,2\rangle$, $\langle 0,2,8,2\rangle$, $\langle 0,3,6,3\rangle$, and $\langle 0,2,8,4\rangle$. The ideal icosahedral cluster $\langle 0,0,12,0\rangle$ is not the most abundant index, but it is within the top 14 and represents more than 2.25% of the entire population. The most prevalent VCs around Zr atoms are $\langle 0,3,6,4\rangle$,

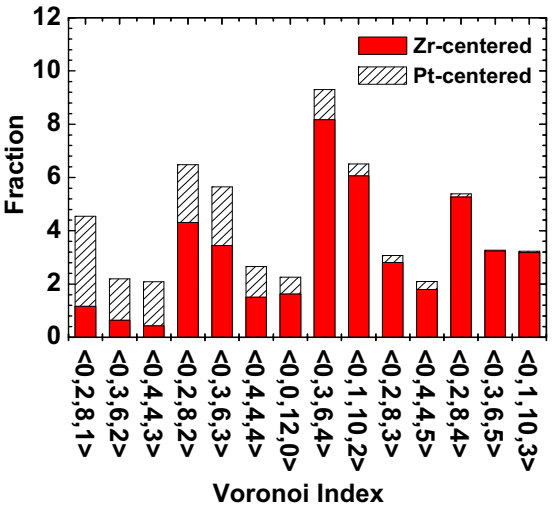

FIG. 6. (Color online) Distribution of Voronoi clusters around Pt and Zr atoms in $Zr_{73}Pt_{27}$ amorphous alloy.

$\langle 0,1,10,2\rangle$, and $\langle 0,2,8,4\rangle$, while the most frequent ones around Pt atoms are $\langle 0,2,8,1\rangle$, $\langle 0,3,6,3\rangle$, $\langle 0,2,8,2\rangle$, and $\langle 0,4,4,3\rangle$. These results reveal that the dominant VCs around the Zr and Pt atoms in the $Zr_{73}Pt_{27}$ glass prefer to have coordination numbers in descending order of 13,14 and 12,11. We note that the relative population of the $\langle 0,0,12,0\rangle$ type cluster in our sample is much smaller than that of the glass $Zr_{84}Pt_{16}$ model proposed by Sheng *et al.*[5] This difference could be partially attributed to the decreased amount of Zr in our $Zr_{73}Pt_{27}$ system. As one can see from Fig. 6, the $\langle 0,0,12,0\rangle$ type cluster has a much stronger preference to form around the Zr atoms than around Pt atoms.

In order to see the character of the SRO within the various types of Voronoi polyhedra in more detail, we calculated the bond-orientational order parameter $\hat{W}_6$ for the center atom of each polyhedron using r_{cut}=3.94 Å. The histograms of these results according to each type of Voronoi indices are shown in Fig. 7. We find that the polyhedrons having the same Voronoi index can have very different $\hat{W}_6$ values. For example, a perfect icosahedral structure is known to have a Voronoi index of $\langle 0,0,12,0\rangle$ and a $\hat{W}_6$ value of −0.169. However, as one can see from Fig. 7, the clusters that have a Voronoi index of $\langle 0,0,12,0\rangle$ exhibit a much broader distribution of $\hat{W}_6$ values. This indicates that $\hat{W}_6$ values are very sensitive to the angular distortions. Nevertheless, the distribution of the $\hat{W}_6$ values from the $\langle 0,0,12,0\rangle$ type clusters can be seen to be distinct from that of other types of Voronoi polyhedra and are weighted on the negative side (i.e., distributed more toward icosahedral symmetry) of the histogram. From the distributions of $\hat{W}_6$ values shown in Fig. 7, we can roughly and somewhat arbitrarily divide the 14 polyhedra into three groups: group A with more icosahedral character, group C with less icosahedral and more cubic character, and group B that has some mixed character in between groups A and C. The clusters belonging to group A are $\langle 0,2,8,2\rangle$, $\langle 0,0,12,0\rangle$, and $\langle 0,1,10,2\rangle$. The clusters belonging to group C are $\langle 0,4,4,3\rangle$, $\langle 0,4,4,4\rangle$, and $\langle 0,4,4,5\rangle$ and those belonging to group B, which are presented on the right-hand

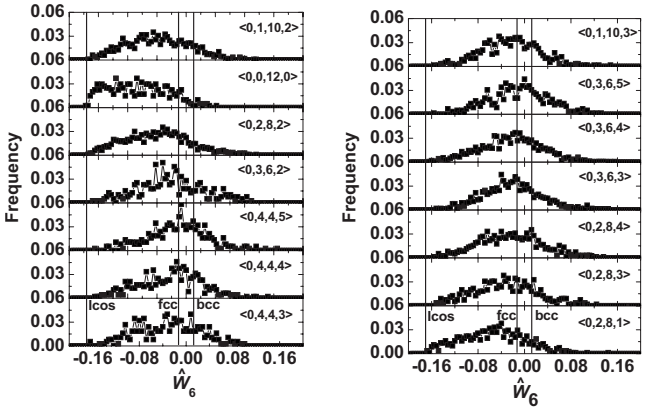

FIG. 7. The calculated frequency density of $\hat{W}_6$ distributions for 14 types of the most abundant polyhedra from Voronoi indexes. The vertical lines indicate the $\hat{W}_6$ values for the ideal icosahedral (−0.169), fcc (−0.013), and bcc (0.013) structures, as indicated in the figure. Note that $\langle 0,0,12,0\rangle$ barely spans the $\hat{W}_6$ value for an icosahedron.

side of Fig. 7, are $\langle 0,2,8,1\rangle$, $\langle 0,2,8,3\rangle$, $\langle 0,2,8,4\rangle$, $\langle 0,3,6,2\rangle$, $\langle 0,3,6,3\rangle$, $\langle 0,3,6,4\rangle$, $\langle 0,3,6,5\rangle$, and $\langle 0,1,10,3\rangle$. The fractions of A, B, and C groups are 15.26%, 39.32%, and 6.84% of the entire population, respectively.

In order to correlate the descriptions of the SRO and better understand how the MRO is constructed the $Zr_{73}Pt_{27}$ glass system, we performed calculations to study the pair-correlation functions among the clusters within groups A–C defined above using the coordinates of the center atoms in each cluster. Since the pair-correlation between random pick of atoms in the sample may also exhibit "first level" atomic correlations, the spatial correlations between the clusters are more clearly seen if we subtract the total pair-correlation function of the whole samples from the pair-correlation func-

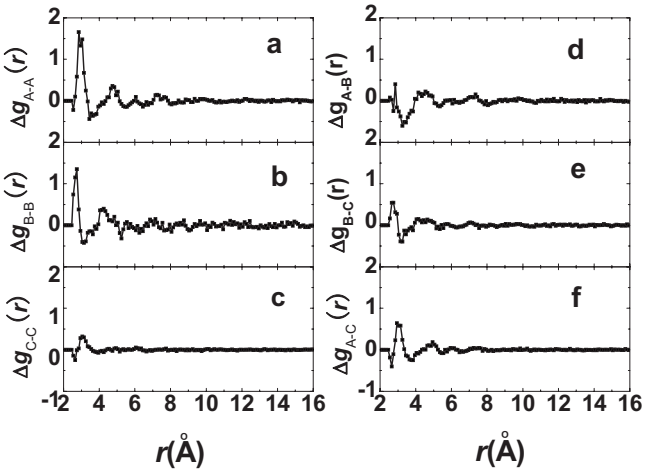

FIG. 8. Difference between the cluster-cluster PCFs $g_{\alpha\beta}(r)$ and the total PCF $g(r)$, i.e., $\Delta g_{\alpha\beta}(r)$, among the cluster belonging to groups A, B, and C, respectively. Clusters in group A are $\langle 0,2,8,2\rangle$, $\langle 0,0,12,0\rangle$, and $\langle 0,1,10,2\rangle$; clusters in group B are $\langle 0,4,4,3\rangle$, $\langle 0,4,4,4\rangle$, and $\langle 0,4,4,5\rangle$; and clusters in group C are $\langle 0,2,8,1\rangle$, $\langle 0,2,8,3\rangle$, $\langle 0,2,8,4\rangle$, $\langle 0,3,6,2\rangle$, $\langle 0,3,6,3\rangle$, $\langle 0,3,6,4\rangle$, $\langle 0,3,6,5\rangle$, and $\langle 0,1,10,3\rangle$.

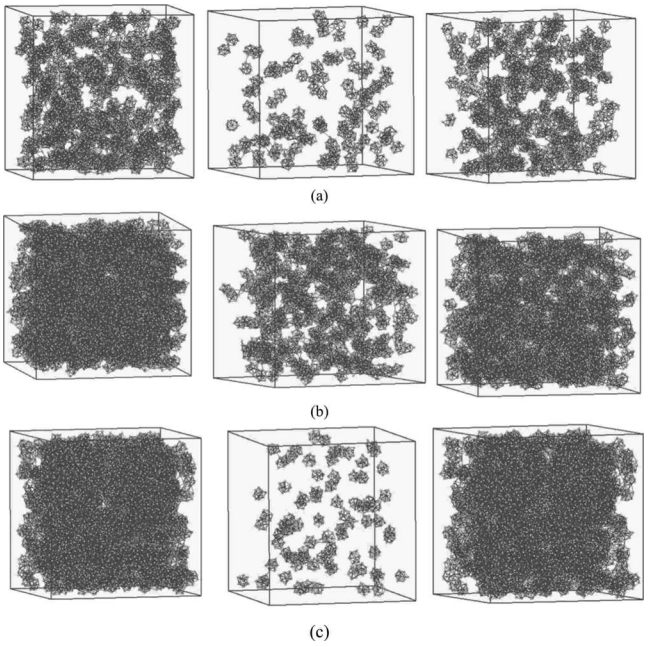

FIG. 9. Distribution of the clusters having Voronoi indices of (a) $\langle 0,0,12,0\rangle$, (b) $\langle 0,2,8,2\rangle$, and (c) $\langle 0,1,10,2\rangle$ (left: total; middle: Pt centered; right: Zr centered).

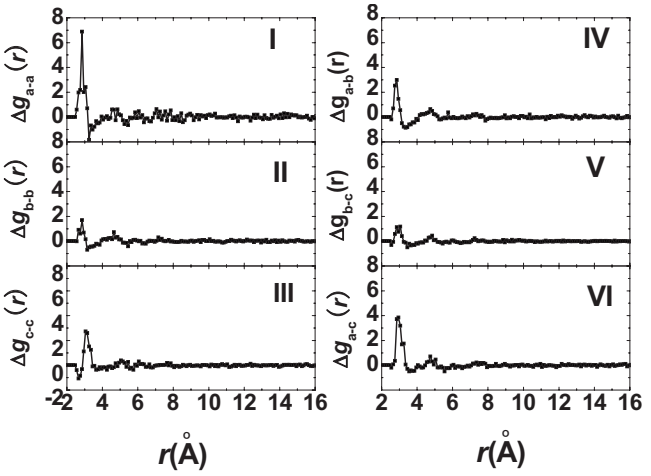

FIG. 10. Difference between the cluster-cluster PCFs $g_{\alpha\beta}(r)$ and the total PCF $g(r)$, i.e., $\Delta g_{\alpha\beta}(r)$, among the cluster belonging to group A (α,β=a,b,c, where a represents $\langle 0,0,12,0\rangle$ clusters, b represents $\langle 0,2,8,2\rangle$ clusters, and c represents $\langle 0,1,10,2\rangle$ clusters).

tions of the particular type of the clusters. The results of the difference between the cluster-cluster PCFs $g_{\alpha\beta}(r)$ and the total PCF $g(r)$, i.e., $\Delta g_{\alpha\beta}(r)$, are plotted in Fig. 8. These correlation functions suggest that the clusters within the icosahedral-like group A have much stronger tendency of being clustering together, while there is almost no correlation between the group C clusters. The correlation of the clusters in group B is slightly weaker than that of group A. In both groups A and B, well cluster packing can be seen up to the second shells.

In Fig. 9, we also show the distribution of the clusters that have Voronoi indices of $\langle 0,0,12,0\rangle$, $\langle 0,2,8,2\rangle$, and $\langle 0,1,10,2\rangle$ (which are the most icosahedral-like of the polyhedra examined) in the glass structure model from the RMC simulation. It is interesting to see that most of the Pt-centered icosahedral-like clusters are the $\langle 0,2,8,2\rangle$ type, while there are very few $\langle 0,1,10,2\rangle$ type Pt-centered clusters in the glass model. The pair-correlation functions [$g_{\alpha\beta}(r)$ and α,β=a,b,c, where a represents $\langle 0,0,12,0\rangle$ clusters, b represents $\langle 0,2,8,2\rangle$ clusters, and c represents $\langle 0,1,10,2\rangle$ clusters] among these icosahedral-like clusters were also calculated using the coordinates of the center atoms in each cluster. The difference between the cluster-cluster PCFs $g_{\alpha\beta}(r)$ of these clusters and the total PCF $g(r)$, i.e., $\Delta g_{\alpha\beta}(r)$, is shown in Fig. 10 which also indicates that the $\langle 0,0,12,0\rangle$ clusters have the strongest correlations among the clusters in this group.

IV. CONCLUSIONS

In summary, we have combined experimental x-ray diffraction data with *ab initio* MD and RMC simulations of an amorphous $Zr_{73}Pt_{27}$ alloy in order to analyze the local structure (i.e., short- and medium-range orders) in glass and liquid states. The calculated structure factors and pair-correlation functions for the glass state are in good agreement with our experimental results. The bond-pair HA analysis of the *ab initio* MD simulations shows that the main HA bond pairs in the liquid and the glass states are 155, 154, and 143. The summation of 155 and 154 pairs increases from 35.8% at T=1850 K to 52.9% as the system is cooled from the liquid to glass, indicating that the icosahedral ordering of the liquid becomes more pronounced during cooling. Furthermore, the fraction of distorted and perfect icosahedra greatly increases in glass state. The icosahedral-like order defining the SRO of the glasses expands as the clusters connect each other to form an icosahedral MRO. The structure of the $Zr_{73}Pt_{27}$ glass was also studied in some details based on the 3D atomistic model generated from the constrained RMC simulations. Analysis of the RMC model structure suggests that the icosahedral-like clusters are packed in arrangements having higher-order correlations, thus establishing medium-range topological order up to two or three cluster shells.

ACKNOWLEDGMENTS

One of the authors (S.Y.W.) was supported by the NSF of China (Grant No. 60578046) and the Fudan High-End Computing Center. Ames Laboratory is operated for the U.S. Department of Energy by Iowa State University under Contract No. DE-AC02-07CH11358. This work was supported by the Director for Energy Research, Office of Basic Energy Sciences, including a grant of computer time at the National Energy Research Supercomputing Center (NERSC) in Berkeley. The work at the Advanced Photon Source was supported by U.S. Department of Energy under Contract No. DE-AC02-06CH11357.

[1] H. Jónsson and H. C. Andersen, Phys. Rev. Lett. **60**, 2295 (1988).
[2] M. Shimono and H. Onodera, Mater. Sci. Eng., A **449-451**, 717 (2007).
[3] T. K. Gu, J. Y. Qin, and X. F. Bian, Appl. Phys. Lett. **91**, 081907 (2007).
[4] W. K. Luo, H. W. Sheng, F. M. Alamgir, J. M. Bai, J. H. He, and E. Ma, Phys. Rev. Lett. **92**, 145502 (2004).
[5] H. W. Sheng, W. K. Luo, F. M. Alamgir, J. M. Bai, and E. Ma, Nature (London) **439**, 419 (2006).
[6] K. F. Kelton, A. K. Gangopadhyay, T. H. Kim, and G. W. Lee, J. Non-Cryst. Solids **352**, 5318 (2006).
[7] J. Saida, M. Imafuku, S. Sato, E. Matsubara, and A. Inoue, J. Non-Cryst. Solids **353**, 3704 (2007).
[8] U. Köster, J. Meinhardt, S. Roos, and H. Liebertz, Appl. Phys. Lett. **69**, 179 (1996).
[9] B. S. Murty, D. H. Ping, K. Hono, and A. Inoue, Acta Mater. **48**, 3985 (2000).
[10] A. Inoue, T. Zhang, J. Saida, M. Matsushita, M. W. Chen, and T. Sakurai, Mater. Trans., JIM **40**, 1181 (1999).
[11] A. Inoue, T. Zhang, M. W. Chen, T. Sakurai, J. Saida, and M. Matsushita, Appl. Phys. Lett. **76**, 967 (2000).
[12] J. Saida, M. Matsushita, and A. Inoue, J. Alloys Compd. **342**, 18 (2002).
[13] L. Q. Xing, J. Eckert, W. Löser, and L. Schultz, Appl. Phys. Lett. **73**, 2110 (1998).
[14] J. Saida and A. Inoue, J. Non-Cryst. Solids **317**, 97 (2003).
[15] J. Saida and A. Inoue, Scr. Mater. **50**, 1297 (2004).
[16] J. Saida, M. Matsushita, and A. Inoue, Intermetallics **10**, 1089 (2002).
[17] M. H. Lee, R. T. Ott, M. F. Besser, M. J. Kramer, and D. J. Sordelet, Scr. Mater. **55**, 505 (2006).
[18] B. Cantor, in *Fundamentals of Rapid Solidification*, NATO ASI Series, Series E: Applied Sciences Vol. 114 (Kluwer Academic, Dordrecht, 1986), p. 3.
[19] T. Egami, J. Non-Cryst. Solids **317**, 30 (2003).
[20] D. B. Miracle, W. S. Sanders, and O. N. Senkov, Philos. Mag. **83**, 2409 (2003).
[21] M. J. Kramer, M. Xu, Y. Y. Ye, D. J. Sordelet, and J. R. Morris, Metall. Mater. Trans. A **39A**, 1847 (2008).
[22] A. P. Hammersley, S. O. Svensson, M. Hanfland, A. N. Fitch, and D. Häusermann, High Press. Res. **14**, 235 (1996).
[23] T. Egami and S. J. L. Billinge, *Underneath the Bragg Peaks: Structural Analysis of Complex Materials* (Elsevier, New York, 2003).
[24] G. Kresse and J. Hafner, Phys. Rev. B **47**, 558 (1993).
[25] G. Kresse, Ph.D. thesis, Technische Universität Wien, 1993.
[26] G. Kresse and J. Furthmüller, Comput. Mater. Sci. **6**, 15 (1996).
[27] G. Kresse and J. Furthmüller, Phys. Rev. B **54**, 11169 (1996).
[28] G. Kresse and D. Joubert, Phys. Rev. B **59**, 1758 (1999).
[29] S. Nosé, J. Chem. Phys. **81**, 511 (1984).
[30] W. G. Hoover, Phys. Rev. A **31**, 1695 (1985).
[31] D. A. Keen and R. L. McGreevy, Nature (London) **344**, 423 (1990).
[32] T. H. Kim and K. F. Kelton, J. Chem. Phys. **126**, 054513 (2007).
[33] R. L. McGreevy and L. Pusztai, Mol. Simul. **1**, 359 (1988).
[34] R. L. McGreevy, J. Phys.: Condens. Matter **13**, R877 (2001).
[35] P. A. Egelstaff, *An Introduction to the Liquid State* (Clarendon, Oxford, 1992), Appendix 4.
[36] D. Waasmaier and A. Kirfel, Acta Crystallogr., Sect. A: Found. Crystallogr. **51**, 416 (1995).
[37] J. D. Honeycutt and H. C. Andersen, J. Phys. Chem. **91**, 4950 (1987).
[38] J. L. Finney, Nature (London) **266**, 309 (1977).
[39] J. L. Finney, Proc. R. Soc. London, Ser. A **319**, 479 (1970).
[40] P. J. Steinhardt, D. R. Nelson, and M. Ronchetti, Phys. Rev. B **28**, 784 (1983).
[41] P. Ganesh and M. Widom, Phys. Rev. B **74**, 134205 (2006).
[42] P. Ganesh and M. Widom, Phys. Rev. B **77**, 014205 (2008).
[43] T. Nakamura, E. Matsubara, M. Sakurai, M. Kasai, A. Inoue, and Y. Waseda, J. Non-Cryst. Solids **312–314**, 517 (2002).
[44] S. Sachdev and D. R. Nelson, Phys. Rev. Lett. **53**, 1947 (1984).
[45] K. F. Kelton, G. W. Lee, A. K. Gangopadhyay, R. W. Hyers, T. J. Rathz, J. R. Rogers, M. B. Robinson, and D. S. Robinson, Phys. Rev. Lett. **90**, 195504 (2003).
[46] T. Schenk, D. Holland-Moritz, V. Simonet, R. Bellissent, and D. M. Herlach, Phys. Rev. Lett. **89**, 075507 (2002).
[47] http://www.tagen.tohoku.ac.jp/general/building/iamp/database/scm/LIQ/gr.html
[48] S. R. Elliott, Nature (London) **354**, 445 (1991).